Compression-After-Impact Strength of Sandwich Panels with Core Crushing Damage

Andrey Shipsha* and Dan Zenkert
Dept. of Aeronautical and Vehicle Engineering
Kungl Tekniska Högskolan
S–100 44, Stockholm, Sweden

Abstract.

Compression-after-impact (CAI) strength of foam-cored sandwich panels with composite face sheets is investigated experimentally. The low-velocity impact by a semi-spherical (blunt) projectile is considered, producing a damage mainly in a form of core crushing accompanied by a permanent indentation (residual dent) in the face sheet. Instrumentation of the panels by strain gauges and digital speckle photography analysis are used to study the effect of damage on failure mechanisms in the panel. Residual dent growth inwards toward the mid-plane of a sandwich panel followed by a complete separation of the face sheet is identified as the failure mode. CAI strength of sandwich panels is shown to decrease with increasing impact damage size. Destructive sectioning of sandwich panels is used to characterise damage parameters and morphology for implementation in a finite element model. The finite element model that accounts for relevant details of impact damage morphology is developed and proposed for failure analysis and CAI strength predictions of damaged panels demonstrating a good correlation with experimental results.

Keywords: impact, impact damage, sandwich panels, foam core, residual dent, crushe core, dent growth, residual strength

1. Introduction

Composite sandwich structures offer clear advantages over other materials in terms of very high bending stiffness at low weight and, therefore, have become extensively used in transportation and infrastructure applications. However, most of sandwich structures, having thin face laminates with low local bending stiffness and low strength of a core material, are inherently susceptible to localized damage when subjected to localized transverse loads. Low-velocity impact by a foreign object (e.g., tool drops, runway debris, bird strikes, etc) is one of common types of localized loads which may induce impact damage and result in reduction of static and/or fatigue strength of sandwich structures. Therefore, understanding the mechanisms of impact damage formation, its morphology and effect on the structural integrity of sandwich structures is important where safety and damage tolerance are primary

* Corresponding author. *E-mail:* andrey@kth.se (A. Shipsha)

concerns, e.g. aerospace and automotive applications. Comprehensive reviews of recent research achievements in the field of impact damage on sandwich structures can be found in Abrate [1] and Tomblin et al. [2].

Depending on the shape and size of an impact object, its mass and velocity, material properties and geometry of a sandwich structure, a number of damage modes can be identified; 1) core crushing, 2) debond at the face-core interface, 3) delaminations and 4) fibre breaks and matrix cracking in face laminates. Compression-after-impact (CAI) strength of sandwich panels with damage confined to the face laminates (delaminations, fiber breaks, etc) has been extensively investigated in many research works [3, 4, 5, 6]. Different models for predicting the CAI strength have been presented and experimentally validated.

For some material configurations, low-velocity impact with a blunt object typically produces a subtle permanent indentation (a residual dent) in the face sheet accompanied with substantial core crushing damage beneath and around the impact site, e.g. Refs. [7, 8, 9]. If a sandwich panel has a relatively brittle core, a debond at the face-core interface may also be produced as a result of rapid rebound of the face sheet upon removal of impact load [10]. The face sheet often remains barely damaged and may mask the core crushing damage from being detected by visual inspections. However, the effect of the core crushing damage on the CAI strength has been shown significant [7, 8, 10].

The aim of this study is to investigate the residual compressive strength and failure mechanisms of foam-cored sandwich panels after low-velocity impact. The focus of this investigation is on the core crushing damage attributed with a permanent residual dent in the face sheet while the laminate itself is considered undamaged. Destructive sectioning of damaged panels is used to characterise damage morphology and determine the key parameters of the impact damage. A finite element model that accounts for relevant details of impact damage morphology is developed and used for failure analysis and CAI strength predictions of damaged panels

2. Experimental study

2.1. Test panels

One sandwich configuration was considered in this study consisting of 2.4 mm quasi-isotropic GFRP faces and 50 mm Rohacell WF51 polymethacrylimide (PMI) foam core. The face sheets were comprised of Devold DBLT600-E10 glass-fibre non-crimp fabric and vinylester Norpol Dion 9500. A large sandwich panel (1.2×1.2 m) was first fabricated

Table I. The mechanical properties of sandwich constituents.

	E_{xx} (MPa)	E_{yy} (MPa)	E_{zz} (MPa)	G_{xy} (MPa)	G_{yz} (MPa)	G_{zx} (MPa)	ν_{yx}	ν_{zx}	ν_{zy}
Core	85	85	85	29.9	29.9	29.9	0.42	0.42	0.42
Face	16500	3800	16500	1800	1800	6600	0.05	0.25	0.25

using the vacuum-assisted resin transfer moulding and then cut into the test panels with in-plane dimensions of 270×180 mm. The mechanical properties of GFRP faces and WF51 foam core are given in Table I. Definition of material axes is shown in Fig. 1.

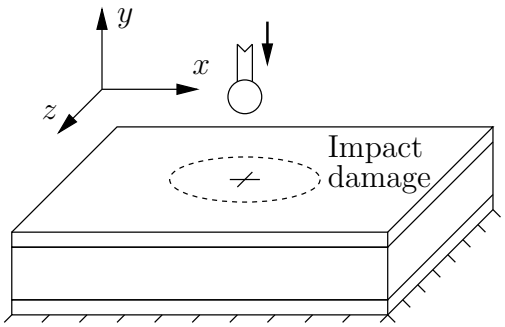

Figure 1. A schematic of the impact test.

2.2. Impact testing

Low-velocity impact tests of sandwich panels were conducted in the drop-weight test rig. An impactor with a semi-spherical tip of 25 mm in diameter and of a total mass of 7.8 kg was equipped with electromagnetic releasing device. The test rig was also instrumented with a load transducer to measure the maximum contact force and load-time response. The deflection of the face laminate under the impactor was registered by means of a laser displacement gauge. Overall bending of the test panels during impact was prevented by an underlying rigid steel plate. After rebound, the impactor was captured to avoid secondary impact of a test panel. The impact energy was varied by changing the drop height of the impactor under assumption of the ideal free fall. A schematic of the impact test is shown in Fig. 1.

Table II. Results from the impact tests (mean values with standard deviation).

	10 J	20 J	30 J	40 J	50 J	60 J
$\bar{P}_{\max}$, kN	2.53	3.67	4.56	5.39	5.98	6.67
	±0.04	±0.07	±0.03	±0.06	±0.10	±0.29
$\bar{\delta}_{\max}$, mm	4.91	6.83	9.30	9.83	10.79	11.88
	±0.16	±0.24	±0.08	±0.12	±0.03	±0.19

Impact energy levels were determined experimentally for the investigated sandwich configuration in order to detect the minimum energy required for producing a barely visible impact damage in the face sheet and the maximum energy that, if exceeded, leads to fibre breaks and penetration of the face sheet. The barely visible damage was first observed in the face sheet after 10 J impact; lower impact energies were producing no visible damage. With increasing impact energy, visual inspection of the panels revealed delaminations in the face laminates confined to the contact area with the impactor. The visible damage size in the face laminate after 60 J impact was about 18 mm in diameter. Further energy increase resulted in distinct fiber breaks and face sheet penetration. Thus, impact energy levels between 10 and 60 J with a 10 J increment were used for producing the dominant core crushing damage. Series of 3-5 panels were tested for each energy level. The values of peak contact force $P_{\max}$ and deflection under impact $\delta_{\max}$ were consistent for the panels tested at the same impact energy level as can be seen in Table II.

2.3. Impact damage characterisation

A profile of the residual dent in the face sheet was measured by means of a dial gauge, in two perpendicular directions across the dent area. The residual dent depth is typically greater by as much as 25-30%, if measured directly after impact testing, owing to significant creep and relaxation effects in the crushed foam core [11, 12]. In this study the measurements of residual dent parameters were conducted 1 hour after the impact testing to ensure that the dent is in a stationary state. Both the depth of the residual dent in the centre, δ_{dent} and the diameter, D_{dent} were increasing with the impact energy. The measurements of the dent diameter D_{dent} along the x- and z-directions, see Fig. 1, indicated that the shape of the residual dent in the x-z plane is circular. For used impact energy range (10–60 J), the residual dent diameter, D_{dent}

varied between 60 and 110 mm while the depth of residual dent, δ_{dent} was between 0.5 and 1.2 mm.

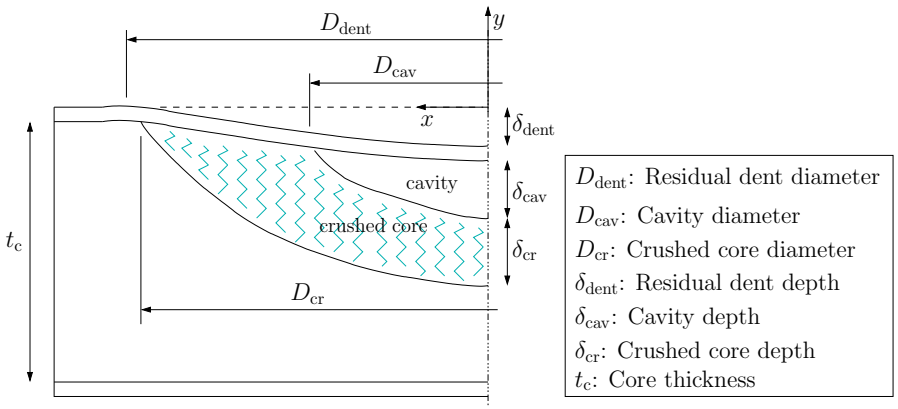

Figure 2. A schematic of the typical impact damage.

Destructive sectioning of one panel from each test series was performed to determine other geometrical parameters which characterise the impact damage and are required for the finite element model. Furthermore, the sectioning of test panels at this stage was necessary to assist with positioning of strain gauges on other panels in the test series which were to be tested in compression. Figure 2 shows a schematic of a typical section cut taken in the x-y plane through the centre of a panel. The geometrical parameters used for characterisation of impact damage are explicitly explained in this schematic. The core crushing damage accompanied by a debond (cavity) between the face and the crushed core was observed in all sectioned panels. Note that standard NDI techniques may be used to determine the residual dent parameters (D_{dent} and δ_{dent}), whereas destructive sectioning is required to measure the core crushing damage characteristics (D_{cr}, D_{cav}, δ_{cr} and δ_{cav}).

In general, all geometrical parameters of damage were increasing with the impact energy while the damage morphology was similar in all panels. It is interesting to note that the residual dent diameter, D_{dent} was only marginally greater than the crushed core diameter, D_{cr} in all sectioned panels. The magnitudes of the cavity depth, δ_{cav} and the crushed core, δ_{cr} were simultaneously increasing with the impact energy while being quite close to each other. Destructive sectioning has also shown that the residual dent depth is much smaller than the total damage depth, i.e. $\delta_{\text{dent}} \ll (\delta_{\text{cav}} + \delta_{\text{cr}})$. For the panels considered in this study, there was no obvious evidence of large scale delaminations in the face sheet.

2.4. Compression-after-impact tests

Displacement-controlled CAI tests of sandwich panels were conducted in a hydraulic testing machine operated at the load rate of 1 mm/min. To avoid local yielding of the faces at the contact with loading platens and to ensure uniform load transfer, the shorter edges of the specimens were tabbed and milled. A dial gauge was used for measuring the out-plane displacements in the centre of the residual dent as shown in Fig. 3(a).

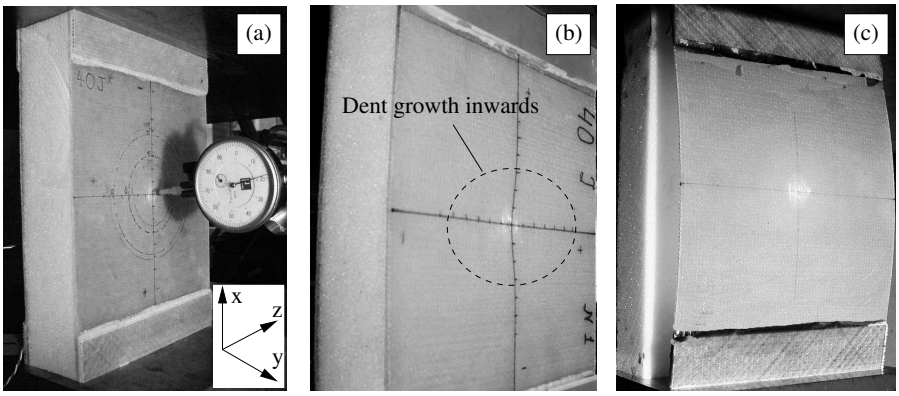

Figure 3. CAI tests of sandwich panels; (a) a test set-up, (b) residual dent growth in the 40 J panel and (c) final failure of the panel.

One test panel from each series was also instrumented with uniaxial strain gauges as shown in Fig. 4. The dashed circles in the figure visualise approximate boundaries of the crushed core and the cavity regions based upon destructive sectioning measurements. A total of eight gauges were used; six gauges were positioned on the impacted face and two gauges on the backside face. Three gauges (SG3, SG4 and SG8) out of six, positioned on the impacted face sheet, along with backside strain gauges (SG1 and SG2) were used to measure far-field strains and to control strain distribution between two face sheets and across the width of the panel. The strain gauge SG5 was located close to centre of the residual dent and over the cavity region. The gauges SG6 and SG7 were positioned along the lines, $x = 0$ and $z = 0$, respectively and over the crushed core region, see Fig. 4. These three gauges were used to investigate the effect of damage on strain distribution in the face sheet.

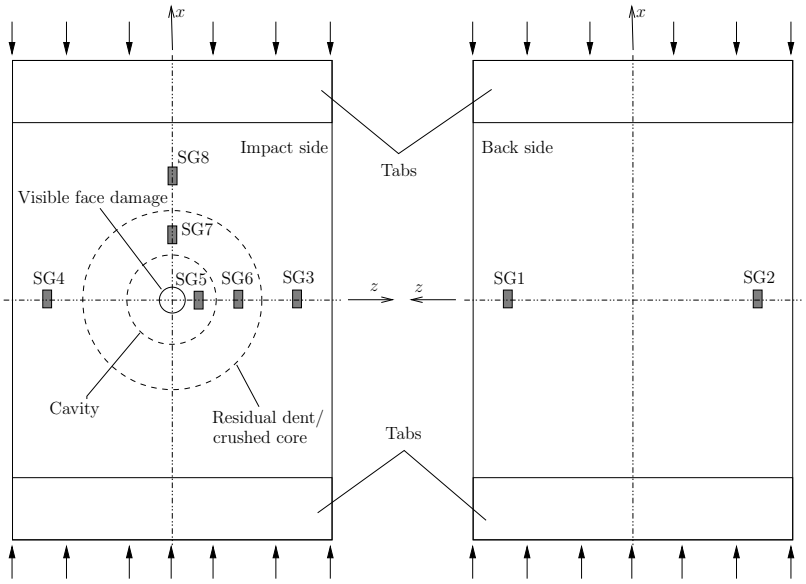

Figure 4. A sandwich panel instrumented with strain gauges.

All tested panels, except for the 10 J panels, exhibited a more or less stable growth of the residual dent inwards toward the mid-plane of the panel preceding the final failure as shown in Fig. 3(b). The growth of the residual dent was registered by the dial gauge and occurred at lower load levels the larger dent was, depending on the impact energy and, consequently, on the damage size. The final failure of the panels was attributed to a complete abrupt separation of the face sheet from the panel followed by a drastic load drop, see Fig. 3(c). A typical load-displacement response from the CAI test is shown in Fig. 5(a). It is interesting to note that the residual dent growth inwards the panel caused only marginal decrease in the panel stiffness and ultimate failure load was noticeably higher than the load corresponding to the onset of the residual dent growth. The load associated with the onset of residual dent growth was determined as the intercept between an extension of the region with stationary dent magnitude (no dent growth) and a tangent to the region of maximum and constant dent growth as shown in Fig. 5(b).

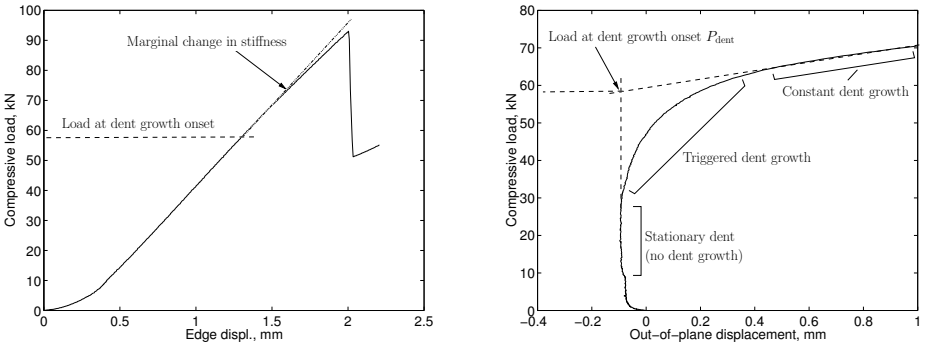

(a) (b)

Figure 5. Results from the CAI tests; (a) a typical load-displacement response and (b) the residual dent growth inwards the panel registered by the dial gauge. The presented graphs are from a 60 J panel test.

Typical strain-load plots from the panels instrumented with strain gauges are presented in Fig. 6. Far-field strains in both impacted (gauges SG3 and SG4) and backside (gauges SG1 and SG2) face sheets were consistent and demonstrated a linear response almost up to final failure, see Fig. 6(a). Ultimate far-field strains at failure were as low as about 0.6–0.65% for 60 J panels and increased with decreasing impact energy, reaching the values about 1–1.1% for the 10 J panels. The responses from strain gauges positioned on the impacted face and over the impact damage are shown in Fig. 6(b). The gauges SG5 and SG6 located over the cavity and the crushed core region, respectively, along the line $x = 0$ (Fig. 4) demonstrated a non-linear response that occurred simultaneously with the onset of dent growth inwards the panel. The strain magnitudes measured by the gauges SG5 and SG6 were greater than the far-field strains due to inwards bending of the face sheet. Simultaneously with the onset of dent growth, the strain gauge SG7 registered a distinct strain decrease attributed to the local bending deformation of the face outwards the panel, see Fig. 6(b). This deformation, seen as "a bulge" in the face sheet, was localised in the region outside the cavity region and along the x-axis, see Fig. 4. The effect of the "bulged" face sheet was even registered by the gauge SG8 which is positioned outside the damaged region, along the x-axis; far-field strains from the gauge SG8 were lower than the far-field strains in Fig. 6(a).

It should be mentioned here that visual observation of the impacted face sheet after CAI tests revealed no evidence of failure caused by compression. Strain levels registered by the strain gauges also suggest that the face laminate was subjected to much lower strains than the ultimate compressive strains for GFRP laminates which are typically

Table III. Results from the CAI tests (mean values with standard deviation).

	Undam.	10 J	20 J	30 J	40 J	50 J	60 J
Onset of dent growth	—	—	77.9	73.6	62.8	57.6	54.4
$\bar{P}_{\text{dent}}$, kN			±6.5	±13.8	±4.2	±2.6	±5.1
Ultimate failure	121.8*	118.5*	117.8	106.9	103.5	96.6	91.3
$\bar{P}_{\text{peak}}$, kN	±2.5	±1.2	±4.5	±4.4	±2.6	±7.7	±7.2

*) Wrinkilng failure

in the order of 2–2.5%. This fact indicates that the failure of damaged panels in CAI testing was most likely initiated somewhere in the foam core.

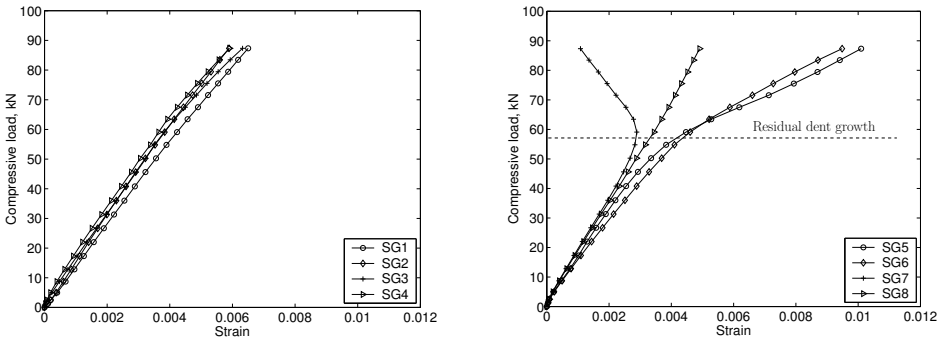

(a) (b)

Figure 6. Results from the strain gauges for a 60 J panel; (a) far-field strains in the impacted and backside faces and (b) strains in the region of impact damage.

The 10 J panels and undamaged panels exhibited classical wrinkling failure in a manner of abrupt bifurcation; the wrinkling wave pattern was well manifested by the foam core which remained on the lower surface of the detached face sheet. No residual dent growth was observed in the panels after 10 J impact prior to ultimate failure. The results from the CAI tests are summarized in Table III. It is important to note that the ultimate strength of 10 J and 20 J panels was almost equal to that of the undamaged panels. The ultimate failure load for the panels which exhibited the residual dent growth preceding the failure was decreasing with increased impact energy and damage size. However, even for the 60 J panels having the largest damage, the CAI strength was only reduced by 25% in comparison with the undamaged panels.

Table IV. Geometrical parameters of the impact damage (mean values with standard deviation).

	10 J	20 J	30 J	40 J	50 J	60 J
D_{dent}, mm	62 ±2.1	79 ±3.9	93 ±4.1	99 ±5.6	104 ±4.5	109 ±3.1
δ_{dent}, mm	0.5 ±0.04	0.7 ±0.05	0.9 ±0.06	1.0 ±0.08	1.1 ±0.07	1.2 ±0.09
D^*_{cr}, mm	60 ±0.5	78 ±1.5	91 ±5.6	97 ±1.6	102 ±4.0	107 ±2.9
δ^*_{cr}, mm	2.9 ±0.4	4.8 ±0.3	5.7 ±0.3	6.4 ±0.9	7.0 ±0.7	8.1 ±0.6
D^*_{cav}, mm	16 ±2.5	21 ±2.4	45 ±4.3	51 ±3.8	56 ±2.9	60 ±3.2
δ^*_{cav}, mm	1.8 ±0.5	3.9 ±0.5	5.4 ±0.7	6.2 ±1.0	7.1 ±0.9	7.8 ±0.9

*) Have to be determined from destructive sectioning

After the CAI tests, the panels were sectioned for measuring the parameters of core crushing damage as shown in Fig. 2. The results of these measurements are summarised in Table IV.

2.5. Digital speckle photography analysis

An optical whole field displacement measurement technique, also known as the digital speckle photography (DSP), was also used in the CAI testing. The DSP method is based on comparison of pairs of digital images taken by a charged coupled device (CCD) camera during the deformation progress [13]. In this study, the DSP system Aramis (GOM mbH, Germany) with two CCD cameras was employed. By using two cameras for imaging the damaged region of a panel from different angles, all three displacement components can be determined. To enhance the DSP measurements, a random pattern was applied on the face sheet surface using white spray paint. At the moment of writing this paper, only one 60 J panel was tested using the DSP analysis.

Figure 7 shows the y-displacement field (out-plane displacement) measured in the damaged region at different load levels. The negative displacement magnitude in the figure corresponds to the displacement inwards the panel. The DSP analysis gave first indication of the residual

dent growth inwards the panel at the load level of approx. 58 kN, see Fig. 7(b). At lower loads, no indication of dent growth could be observed. After the onset of dent growth, the dent has developed inwards the panel in a stable manner until a catastrophic failure occurred at the load level of approx. 95 kN, see Fig. 7(d). The growth of the residual dent during the CAI testing can be also studied through the dent profile plots as shown in Fig. 8. There are four dent profiles presented in the figure that correspond to the images shown in Fig. 7.

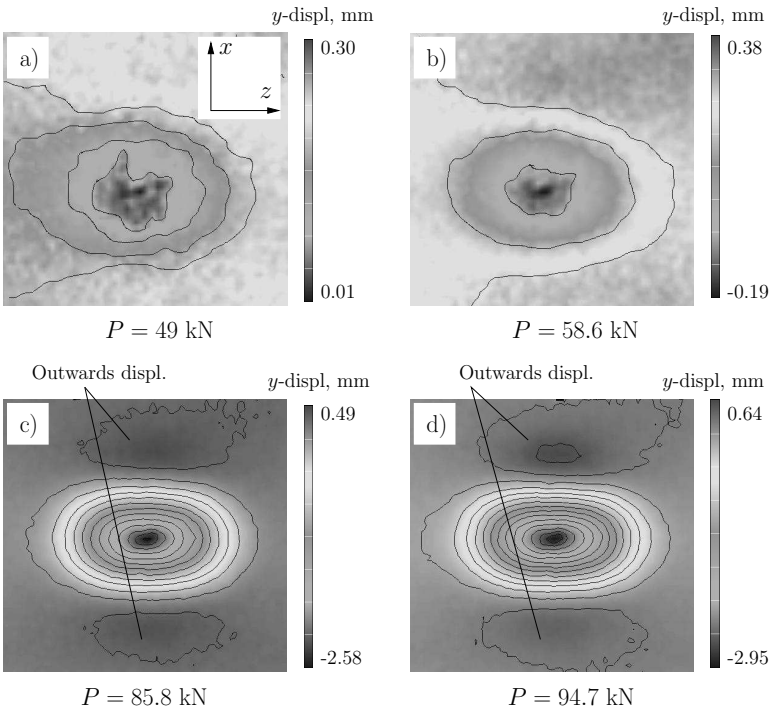

Figure 7. Out-plane displacements around the residual dent obtained by the DSP analysis. The panel was loaded in x-direction. The lines in the images are isolines for the y displacement.

As mentioned previously, no evidence of damage caused by compressive loading was found in the face sheet separated from a panel as a result of final failure. Furthermore, the strains in the face sheet (Fig. 6) also suggest that the failure of the panel may possibly be initiated somewhere in the core or near interface. Visual observations of the separated face sheet revealed traces of the foam core just at the outer boundary of the core crushing damage indicating a possible origin of the failure. A rational hypothesis for a failure mechanism of investigated panels can be attributed to the out-plane tensile fracture of the foam core in the zones with outwards displacements as schematically shown in Fig. 9.

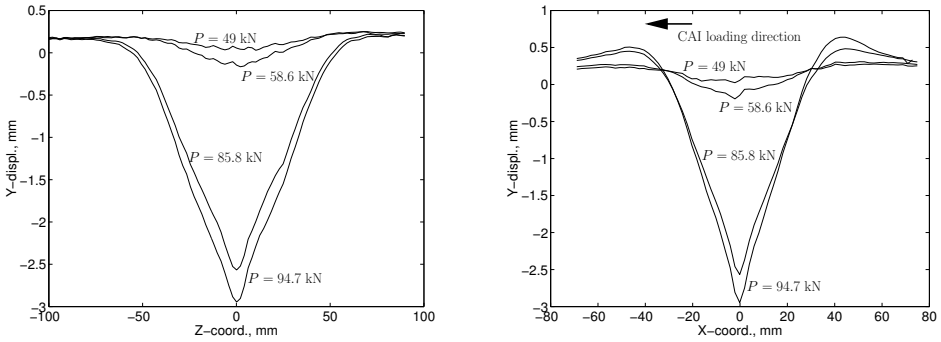

(a) (b)

Figure 8. Residual dent profiles from the DSP analysis; (a) along the z-axis (transverse to the load) and (b) along the x-axis (in the loading direction).

This hypothesis is somehow supported by the DSP analysis where the zones with positive (outwards) y-displacements of the residual dent could be clearly seen, see Fig. 7(c,d) and Fig. 8(b). The displacement magnitude in these zones was increasing simultaneously with the residual dent growth inwards and just before the final failure it was about 0.64 mm corresponding to approximately 1.3% nominal tensile strain in the foam core. This strain is in the same order of magnitude as the tensile fracture strain for undamaged WF51 core material. However, the "bulged" regions appear mostly in a region of crushed foam core where local stress cannot be measured by means of any system used in this study. The residual tensile strength of crushed WF51 foam was previously measured [12] and is approximately 0.15-0.25 MPa.

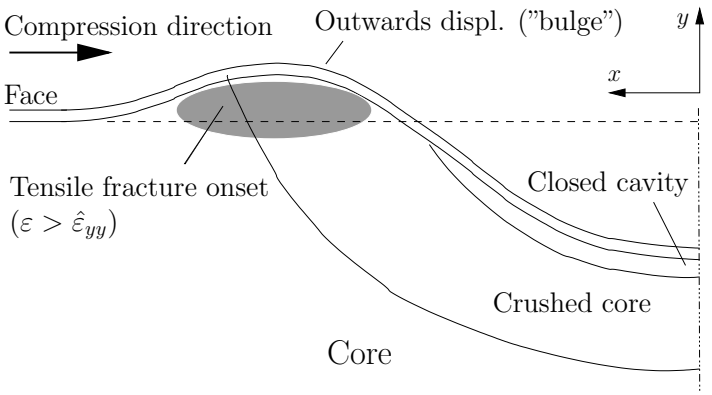

Figure 9. The hypothesis of the failure mechanism in the investigated panels.

3. Numerical modelling of impact damage

3.1. Finite element model

A three dimensional (3D) finite element (FE) model of a sandwich panel of the same size as used in the CAI testing (270×180 mm in plane) was developed using the FE package ABAQUS [14]. The faces and the core were explicitly represented in the FE model using geometry and material properties as given in section 2.1 and Table I. Detailed parametrised representation of the impact damage was implemented in the FE model based on results from destructive sectioning. In particular, the geometry of the crushed core zone containing the cavity was modelled as illustrated in Fig. 2. The residual dent profile was approximated as a function of radial distance from the centre of impact damage using a third degree polynomial. The crushed core and the cavity profiles were represented using a second degree polynomials. From symmetry, only one-fourth of a sandwich panel was modelled as shown in Fig. 10. A Cartesian coordinate system was used with the origin in the centre of the damage. The x-axis corresponds to the direction of the CAI loading. Symmetry boundary conditions were imposed in the model and a compression load was applied as a prescribed displacement at the edge.

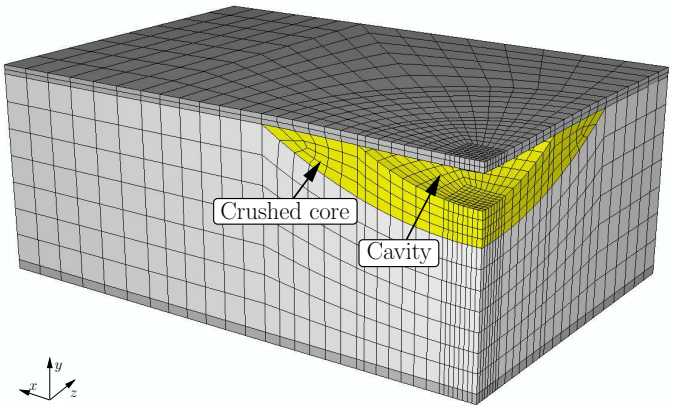

Figure 10. FE model of the sandwich panel with impact damage.

The FE mesh was refined towards the centre of the damage to account for large elastic face sheet deformations as well as for non-linear material response of the crushed core. In the previous studies [10, 12], it was shown that the compressive response of the crushed WF51 foam resembles the compressive response of the virgin foam but having much lower elastic Young's modulus, $E_y = 7.5$ MPa, and yield stress, $\sigma_y = 0.1$ MPa. In the FE analysis, the response of the crushed core

was simulated using the *CRUSHABLE FOAM material model [14]. This material model was calibrated using the test data from a uniaxial compression test of the crushed foam core [12].

Four FE model configurations representing the panels which exhibited the residual dent growth prior to final failure, i.e. 20–60 J panels, were considered in the FE analysis. The damage parameters in the FE configurations were chosen based on the on the physical damage parameters (see Table IV). The FE configurations are summarised in Table V. Non-linear load-displacement FE analyses were carried out for the developed models using Riks method.

Table V. Finite element models.

Parameters	M80	M90	M100	M110
D_{dent}, mm	80	90	100	110
δ_{dent}, mm	0.8	1.0	1.1	1.2
D_{cr}, mm	80	90	100	110
δ_{cr}, mm	5.0	6.0	7.0	8.0
D_{cav}, mm	30	50	60	60
δ_{cav}, mm	5.0	6.0	7.0	8.0

3.2. Finite element results

A typical plot of the out-plane displacement of the residual dent as a function of the applied load is presented in Fig. 11(a). The presented curve is taken from the analysis of the M110 model corresponding to the 60 J panel, see Table V. For comparison, two relevant experimental curves for 60 J panels obtained using the dial gauge and the DSP analysis are plotted in the same graph. In general, the FE model provides a fair representation of the residual dent behaviour. However, a stationary residual dent condition, seen in the experimental curves, is not represented by the FE analysis. This can be attributed to the fact that the residual stresses, typically present in the crushed core due to elastic face sheet, were not accounted for in the FE model.

The predicted and experimentally measured strains plotted as a function of applied load are compared in Figure 11(b). The comparison of predicted and experimentally measured far-field strains demonstrated very good agreement. Also, the strains that correspond to the location of the strain gauge SG7, Fig. 4, are numerically evaluated in the FE analysis and plotted against experimental curves. As shown in the experimental part of this study, a strain response in the location of

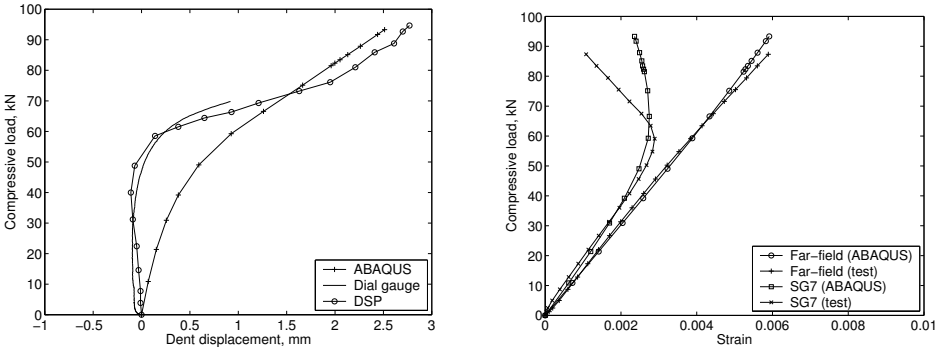

(a) (b)

Figure 11. Comparison of the results from FE analyis and experiments; (a) predicted and experimentally obtained residual dent growth inwards the panel and (b) predicted and experimentally measured strains.

the gauge SG7 can provide an indication of the onset of residual dent growth inwards the panel. The predicted strains showed a quite fair comparison with the results obtained from the strain gauge SG7.

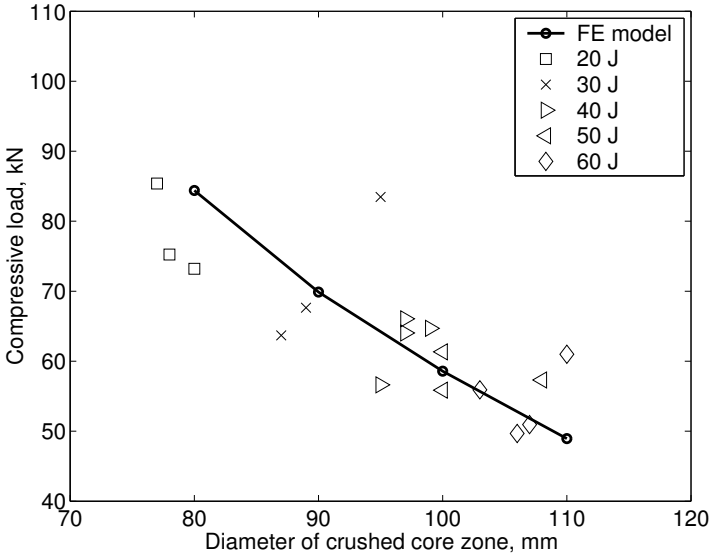

Figure 12. A comparison of predicted and experimentally determined loads for the onset of the residual dent growth.

This feature of the FE analysis was used to estimate the loads at the onset of residual dent growth. The SG7 strains were plotted against the applied load for all four FE models, see Table V. The load corresponding to the onset of dent growth was obtained from these plots as

the intercept between two tangent lines, similar to a technique used in the experimental part. The estimated loads at the dent growth onset are compared with experimental values from Table III and plotted in Fig. 12. The FE predictions gave a good correlation with experimental results.

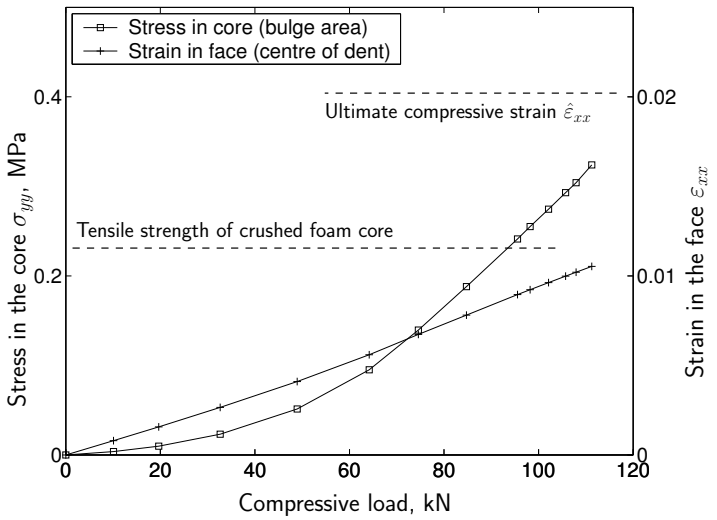

Figure 13. Estimated tensile stresses in the crushed core and compressive strains in the dent centre.

As mentioned earlier, the final failure of the damaged panels could possibly be attributed to the out-plane tensile fracture of the foam core in the zones above and below the residual dent. The FE model was used in an attempt to verify this hypothesis. During the residual dent growth inwards the panel, there are two competing failure mechanisms which may trigger the final failure. These are the tensile failure of the crushed core in the bulged regions, see Fig. 9, and the compressive failure of the face laminate in the centre of the dent, where the compressive strains and stresses have a maximum. In both cases, the stresses and strains exhibit a non-linear behaviour with the load in the CAI test. The core tensile stress is typically very small prior to any significant dent growth, but as the dent magnitude increases, the out-plane stresses σ_{yy} will increase rapidly. In the face sheet, the total compressive strain is a superposition of the applied far-field compressive strain and the bending strain occurring from the dent growth. The latter will initially be small, but will increase with the dent growth inwards the panel. Figure 13 shows the FE estimates of the maximum tensile core stress σ_{yy} (in the crushed core) and the maximum compressive strain in the centre of the dent as function of the applied load. From the graph, it is clear that

the stresses in the crushed core (the bulged region) reach the ultimate values of 0.15-0.25 MPa [12] whereas the compressive strains in the centre of the dent still remain clearly below the ultimate compressive strains (2-2.5% for GFRP laminates). The experimentally measured strains at the dent centre are only about 1%, see Fig. 6(b). Of course, it can be argued that for other material configurations the situation could be reversed plausibly. Anyway, the failure mode occurring in the tests is verified with the FE analysis and furthermore, the FE analysis seems to be capable to estimate the failure loads providing the accurate material properties of the crushed core are measured and available.

4. Conclusions

Experiments showed that the impact damage reduces the compressive strength of the panels, albeit this reduction was not so significant. The residual dent growth inwards the panel followed by a complete abrupt separation of the face sheets was identified as the failure mode. Destructive sectioning and visual observations of failed panels suggested that the failure mechanism could possibly be attributed to the out-plane tensile fracture of the foam core in the bulged regions as the impacted face sheet provided no evidence of compressive failure.

The physically motived FE model that account for relevant details of the impact damage morphology was developed for the analysis of CAI strength of sandwich panels with core crushing damage. A comparison of the numerical results with experiments demonstrated that the FE model provides a fair representation of the damaged panel behaviour in compression with respect to the residual dent growth and strain distribution. The FE model was also shown capable to estimate failure loads providing that crushed core properties are accurately determined.

In general, this investigation demonstrates that the finite element analysis have a potential to provide accurate simulation of a behaviour of damaged panels in compression provided that the damage parameters and damage configuration can be characterised (NDI, destructive sectioning, etc).

Acknowledgements

The authors gratefully acknowledge the Office of Naval Research (ONR) for financial support provided through the program officer Dr. Y.D.S. Rajapakse. Mr. V. Koissin is greatly acknowledged for assistance with experiments. Special thanks go to Röhm GmbH & Co. KG of Darmstadt, Germany for supplying the Rohacell WF51 foam core.

References

1. Abrate S., 'Localised Impact on Sandwich Structures with Laminated Facings', *Applied Mechanics Reviews* **50**(2), 1997, 69–82.
2. Tomblin, J., Lacy, T., Smith, B., Hooper, S., Vizzini, A. and Lee, S., 'Review of Damage Tolerance for Composite Sandwich Airframe Structures', Federal aviation administration report No. DOT/FAA/AR–99/49, 1999.
3. Kassapoglou, C., Jonas, P.J. and Abbott, R., 'Compressive Strength of Composite Sandwich Panels After Impact Damage: An Experimental and Analytical Study', *Journal of Composite Technology and Research* **10**(2), 1988, 65–73.
4. Caprino, G. and Teti, R., 'Impact and Post-Impact Behaviour of Foam Core Sandwich Structures', *Composite Structures* **29**, 1994, 47–55.
5. Wu, C.L. and Sun, C.T., 'Low Velocity Impact Damage in Composite Sandwich Beams', *Composite Structures* **34**, 1996, 21–27.
6. Davies, G.A.O., Hitchings, D., Besant, T., Clarke, A. and Morgan, C., 'Compression After Impact Strength of Composite Sandwich Panels', *Composite Structures* **63**, 2004, 1–9.
7. Lacy, T.E. and Hwang, Y., 'Numerical Modelling of Impact-Damaged Sandwich Composites Subjected to Compression-After-Impact Loading', *Composite Structures* **61**, 2003, 115–128.
8. Horrigan, D.P.W. and Aitken, R.R., 'Compressive Loading of Composite Sandwich Panels After Impact Damage', *Fifth International Conference on Sandwich Construction*, Zurich, Sept. 5–7, 2000.
9. Horrigan, D.P.W., Aitken, R.R. and Moltschaniwskyj, G., 'Modelling of Crushing Due to Impact in Honeycomb Sandwiches', *Journal of Sandwich Structures and Materials* **2**(2), 2000, 131–151.
10. Shipsha, A., Hallström, S. and Zenkert, D., 'Failure Mechanisms and Modelling of Impact Damage in Sandwich Beams—A 2D approach: Part I—Experimental Investigation', *Journal of Sandwich Structures and Materials* **5**(1), 2003, 7–32.
11. Zenkert, D., Shipsha, A. and Persson, K., 'Static Indentation and Unloading Response of Sandwich Beams', *Composites Part B* **35**(6–8), 2004, 511–522.
12. Koissin, V. and Shipsha, A., 'Crushing behaviour of foam cores in uniaxial compression-tension-compression cycle', *to be presented at the Seventh International Conference on Sandwich Structures*, Aalborg, August 29–31, 2005.
13. Melin, G., 'Optical Whole Field Measurement Techniques for Mechanical Testing — A Review', The Aeronautical Research Institute (FFA), technical report No.FFA TN 1999–35, 1999.
14. ABAQUS 6.4, Hibbit, Karlsson and Sorensen, 2003.
15. Shipsha, A., Hallström, S. and Zenkert, D., 'Failure Mechanisms and Modelling of Impact Damage in Sandwich Beams—A 2D approach: Part II—Analysis and Modelling', *Journal of Sandwich Structures and Materials* **5**(1), 2003, 33–52.